High-resolution Lidar Experiment for the Thirty Meter Telescope

Thomas Pfrommer[a], Paul Hickson[a], Chiao-Yao She[b] and Joseph D. Vance[b]

[a]University of British Columbia, 6224 Agricultural Road, Vancouver V6T1Z1, BC, Canada;
[b]Colorado State University, Fort Collins 80523-1875, CO, USA

ABSTRACT

Adaptive optics (AO) systems of next generation optical ground telescopes will employ laser guide stars (LGS) to achieve wide sky coverage. In these systems the mesospheric sodium layer at $\sim$ 90 km height is excited by means of laser-induced fluorescence of the Na I D_2 resonance hyperfine transmission. The finite thickness of sodium layer, and temporal variations in its density structure, result in LGS that are elongated and have internal structure that varies with time. This degrades the performance of the AO system due to degeneracy between effects of atmospheric and sodium layer variations. In order to quantify this and assess the impact on future extremely large telescopes such as the Thirty-Meter Telescope (TMT), measurements are needed of the density distribution of the sodium layer with high spatial and temporal resolution.

We describe the design of a new lidar experiment to investigate the spatio-temporal power spectra of the Na-variations at frequencies as high as 50 Hz. This system employs a 5 W pulsed laser and a 6 m liquid mirror telescope, which provide sufficient sensitivity for high-resolution studies. The transmitter is a YAG-pumped dye laser, with an optical collimation system that allows the beam divergence to be controlled over a range from diffraction-limited to several arcmin. This will also allow the investigation of saturation effects, important for the next generation high power LGS systems. Backscattered photons will be collected at the prime focus using four high-efficiency photomultiplier detectors and a fast counting system. The resulting system will provide vertical density profiles with a spatial resolution as small as 2 m.

Keywords: Adaptive optics, sodium layer, lidar

1. INTRODUCTION

Next-generation extremely large telescope are being designed to achieve diffraction-limited image quality. To mitigate atmospheric distortions that prevent any telescope with diameter D from achieving diffraction limited resolution $\vartheta \approx \lambda/D$, AO systems are employed. An AO system senses the phase distortion introduced by the atmosphere and corrects it by means of deformable mirrors. Since the atmospheric phase distortion changes on a short timescale, typically a few milliseconds, corrections must be made at several hundred Hz. The required phase information can be derived from light received by the telescope from one or more reference stars located near the object, or in the field of interest. However in most cases there are no stars of sufficient brightness available close enough to the object being observed (the "science target"). For this reason, the TMT AO systems will use artificial stars, created by illuminating the atmospheric sodium layer using a laser. These "laser guide stars" (LGS) are cylinders of resonant-fluorescent sodium atoms which, when seen from the telescope, appear star-like (or slightly elongated) with a minimum angular size, set by atmospheric turbulence, on the order of an arcsec.

A problem arises, however, because the sodium layer is extended in height. When seen from most points in the entrance pupil of the telescope (normally the primary mirror), the LGS appears elongated because of horizontal separation between the laser launch telescope and the observation point causes the cylinder of illuminated sodium atoms to be viewed obliquely. LGS elongation reduces the accuracy with which the centroid of the image can be determined, and also introduces systematic errors if the mean, intensity weighted, height of the sodium varies. Such changes can arise from fluctuations in the density distribution of sodium atoms within the layer or when new material is brought in from sublimating meteoroids.

Correspondence: pfrommer@phas.ubc.ca

A second problem arises because changes in the mean height of the sodium cause the LGS images to defocus slightly. The AO system cannot distinguish between defocus caused by the atmosphere and defocus caused by variations in the sodium mean height, making it impossible to keep the science target in focus. For this reason (and another: LGS cannot sense atmospheric "tip-tilt" fluctuations that change the position of the science target) it is essential that NGS also be employed. The available stars are generally very faint, sufficient only to provide the lowest order phase information (tip-tilt and focus). Because of this, the focus signal is noisy and has insufficient time resolution to allow the AO system to distinguish perfectly between focus errors caused by the atmosphere and those caused by variations in the sodium height. Therefore, variations in the sodium height, if sufficiently large on small timescales, can cause a significant loss of performance of the AO system.

Initial estimates of the power spectrum of sodium height fluctuations have been made by Davis et al.[1] who find that it is well represented by a power law, at least at frequencies below 3 mHz. Herriot et al.[2] estimate that if this power spectrum continues to high frequencies it will contribute significant variance to the residual wavefront error of the TMT Narrow-Field Infrared Adaptive Optics System (NFIRAOS).[3] Because the extrapolation of the low-frequency power law over 6 orders of magnitude to frequencies as high as 1 kHz is highly uncertain, it is possible that sodium height fluctuations will not be a concern. But, it is also possible that they could pose a serious problem for AO systems of the TMT and other extremely large telescopes. For this reason it is essential to determine the temporal behaviour of the sodium density profile at higher frequencies, close to those of the atmospheric focus fluctuations. This is the primary aim of the LZT lidar project.

AO systems employing pulsed lasers have the potential to overcome some of the limitations imposed by the finite thickness of sodium layer. By tracking a pulse as it travels upward through the layer, the LGS position and focus can in principle be corrected continuously. Radial-format CCDs could shift photoelectrons rapidly to follow the transverse motion of the LGS as the laser pulse propagates upward, thus defeating LGS elongation. Dynamic refocusing can correct for the change in range to the LGS during propagation. In pulsed laser systems, the luminous energy is concentrated into a pulse of short duration. The instantaneous energy density is thus much higher than in continuous wave (cw) systems. Because of this, and the need to focus the beam to reduce the angular divergence as much as possible, typically to an arcsecond or smaller, saturation of the sodium atoms becomes a potential issue. Saturation occurs when a large fraction of the sodium atoms are excited to the upper state of the transition by the laser photons, reducing the number of atoms in the ground state. Since the cross section for absorption of laser photons is proportional to the number of atoms in the ground state, the efficiency drops as many laser photons propagate upward without being absorbed. This limits the return flux from the LGS. This effect needs further study and analysis to quantify the potential impact on future TMT AO systems.

To address the above-mentioned issues, the main objectives for the UBC lidar system are:

- Measure the vertical density profile of the sodium layer with a temporal resolution of 50 Hz and a vertical resolution of 5 m or better.
- Determine the spatio-temporal power spectra of the density variations and assess the degree to which match-filtering type centroiding of elongated LGS can provide improved performance.
- Determine the temporal power spectrum of the mean (intensity weighted) height and assess the performance impact of these fluctuations on NFIRAOS.
- Model Na saturation effects and confirm the results by direct observations. (This is a secondary goal to support future TMT AO systems)

In the following sections, we will describe the design of a lidar system capable of detecting sodium-layer variations in the 50 Hz range as well all other outlined objectives.

2. THEORY

2.1 Effect of Na-height Variations on Wavefront Error

Light propagating from a LGS at distance z along the line of sight produces spherical wavefronts with radius of curvature z reaching the telescope. When correctly focused, the telescope optics transmits this light to the LGS

wavefront sensor (WFS) entrance pupil as a plane wave (assuming perfect optics and no atmospheric turbulence). If now the distance to the LGS changes by a small amount Δz, with no refocusing, the wavefront arriving at the WFS acquires a small curvature. The RMS optical path difference between this wavefront and the original plane wave (averaged over the pupil with the piston term removed) is given by[1]

$$\sigma_f = \frac{1}{16\sqrt{3}} \frac{D^2}{z^2} \Delta z \,. \tag{1}$$

The effect of this variation on the wavefront error of the science image produced by the AO system can be estimated as follows. Let $P_\nu(\nu)$ be the temporal power spectrum of the mean height of the sodium and ζ be the zenith angle of the LGS ($z = h \sec\zeta$). Let $H_\nu(\nu)$ be the residual transfer function of the AO system to LGS focus errors. Then, the residual wavefront variance is given by

$$\sigma_{fr}^2 = \frac{1}{768} \frac{D^4}{h^4 \sec^2\zeta} \int_0^\infty |H_\nu(\nu)|^2 P_\nu(\nu) d\nu \,. \tag{2}$$

Davis et al. have estimated the power spectrum of mean height variations from data obtained with the Colorado State University (CSU) lidar system. This system has a sampling frequency of approximately 2 min and a vertical resolution of 150 m. Thus, it is possible to determine the power spectrum over a frequency range of 10 μHz to 3 mHz. From an analysis of 28 nights of CSU lidar data, Davis et al. find following functional form:

$$P_\nu(\nu) = 10^\beta \nu^\alpha \, \mathrm{m^2 Hz^{-1}} \,, \text{where} \quad \alpha = -1.79 \pm 0.02 \;\text{ and }\; \beta = 1.12 \pm 0.40 \,. \tag{3}$$

Herriot et al.[2] describe a "blended" AO control algorithm, where they combine low-frequency focus information from the NGS with higher frequency information from the LGS in order to optimize performance. Using the above sodium power spectrum, they estimate a median residual RMS wavefront error of 24 nm and a 90th percentile error of 63 nm, which is a significant portion of the overall error budget.

A major source of concern is the fact that the power spectrum was measured at frequencies below 3 mHz, yet the residual transfer function has most of its response above 10 Hz. The required extrapolation of the power spectrum over some four orders of magnitude in frequency is a significant source of uncertainty and risk. Direct measurements of the power spectrum at frequencies greater than 20 Hz will help to mitigate this problem.

2.2 Lidar Basics

A sodium lidar uses a pulsed laser to excite the Na D_2 resonance hyperfine transition at 589 nm ($^2P_{\frac{3}{2}} - {}^2S_{\frac{1}{2}}$). Radiated photons are collected by a telescope and registered by a high-speed photon counting detector. Since the lifetime τ of the excited state is short ($\sim$16 ns), the time lag t between pulse transmission and reception gives the range to the emitting atom $z = t/2c$, where c is the mean speed of light on the atmosphere. The number of backscattered photons, detected at a distance z in an interval dz is given by

$$dN_S(z) = \left[\int \left\{ \frac{P_L(\lambda)\Delta t \lambda}{hc} \cdot \eta_{tr} \cdot \sigma_{eff}(\lambda, z) n_{Na} \cdot \frac{A_{tel}}{4\pi z^2} \cdot T_{atm}^2(\lambda) \cdot \eta_{rec} \right\} d\lambda + \frac{q_B}{2c} \right] dz \,. \tag{4}$$

$P_L(\lambda)$ is the fraction of laser power in the wavelength interval from λ to $\lambda + \Delta\lambda$ (units $\mathrm{nm^{-1}}$), radiated within one laser pulse of length Δt, η_{tr} represents the transmitter efficiency, including all optics transmittances, $\sigma_{eff}(\lambda, z)$ is the effective resonant scattering cross section of one sodium atom at height z, n_{Na} is the volume density of sodium atoms, taken within a layer of thickness Δz. A_{tel} represents the effective collecting area of the telescope and $T_{atm}(\lambda)$ is the transmittance of the atmosphere. The receiver efficiency η_{rec} includes all transmittances/reflectivities from all receiver optics, telescope obscuration and detector quantum efficiency. Background counts from dark current and electronics noise are represented by q_B, the dark counts per unit time. For our zenith telescope, height h and distance z are equal.

To determine the wavelength dependent laser power with the absorption cross section, the hyperfine structure (see Figure 1) of the D_2-line is needed. The interaction of the nuclear spin of the Na atom with the electronic shell splits the $^2P_{\frac{3}{2}}$-level into 4 energy levels and the ground level $^2S_{\frac{1}{2}}$ into 2 energy levels. Thermal motion

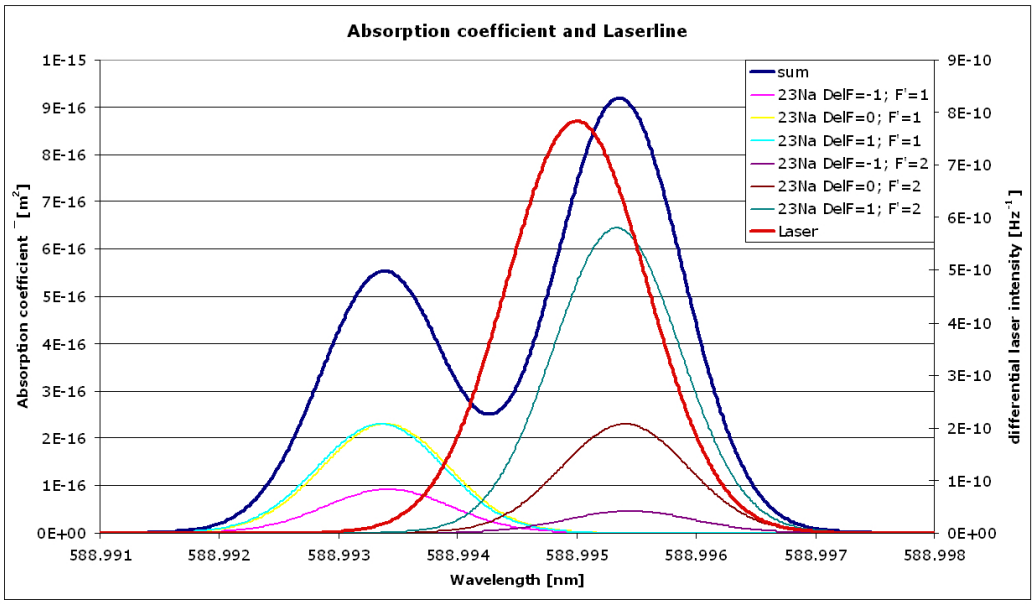

Figure 1. Hyperfine structure of the Sodium D_2-line and resulting line for a temperature of 200 K, comparable to conditions at 90 km height. The laser line, used for the current setup, in red is also shown.

($T_{atm} \sim 200$ K at 90 km height) of the sodium atoms broadens the line to a width of approximately 2.5 Ghz.[4] Atmospheric physicists use narrowband lasers to probe the line shape, thereby extracting information about temperature, wind velocity, etc. For our purpose, we want only to maximize the number of returned photons. If the laser line width is smaller than the Na line width, Na atoms with line-of-sight velocities that put them outside the laser line will not be excited. As there are fewer Na atoms to be potentially excited, saturation will occur more easily. Conversely, if the laser line width is greater than the Na line width, photons with wavelengths outside the Na line will not excite sodium atoms. The best strategy for avoiding saturation and still getting the maximum photon flux, is to match the laser line width to the intrinsic Doppler broadened Na line width. This implies a line width of order 1 or 2 Ghz for the laser, taking into account the difficulty of controlling the intrinsic laser wavelength within 1 GHz (corresponding to 1 pm at 589 nm).

With a high-efficiency detector, the predominant noise will be due to photon statistics. Equation (4) can be inverted to give the sodium volume density in one bin. Ignoring background counts, the 1σ uncertainty in the log of this density is

$$\sigma\{\ln[n(z)]\} = \frac{1}{\sqrt{N(z)}}\,. \tag{5}$$

The uncertainty can be reduced by averaging over multiple shots, but at the expense of a corresponding loss in temporal resolution. The CSU data, from which the power spectrum of Equation (3) was derived, result from averaging of 6000 laser shots taken at a rate of 50 Hz. Our aim is to increase the signal-to-noise ratio without degrading the temporal resolution. This will be achieved by a combination of two factors:

- Increasing A_{tel}, the collecting area of the telescope, the detector quantum efficiency and the throughput of the receiver optics and thereby the number of photons detected.
- Employing averaging in the Fourier domain.

The details of this approach are described in Section (4).

3. SYSTEM DESIGN

The lidar system uses a pulsed laser, a launch telescope and beam steering mirror to project a collimated beam vertically through the atmosphere. Backscattered photons are collected by a 6 m liquid mirror telescope, described below, which directs the light to the lidar receiver located at the telescope prime focus. The overall system design is illustrated in Figure 2. Some details of the main subsystems are provided below.

3.1 The Liquid-Mirror Telescope

The Large Zenith Telescope (LZT) is a fixed, zenith-pointing telescope employing a 6.0 m diameter rotating liquid primary mirror.[5] The rotation period of the mirror is 8.5051 s, which gives a focal length of 9.0 m. A film of mercury, with an average thickness of 1.5 mm, forms the reflecting surface. A thin (12.5 μm) film of Mylar stretched over the mirror protects the mercury surface from wind. Light focused by the primary mirror passes through a four-element refracting corrector that gives seeing-limited image quality over a 22 arcmin diameter field of view. The final focal ratio is 1.67 and the effective focal length is 10.0 m. The corrector is mounted on a focusing stage that compensates for thermal expansion and contraction of the telescope structure. Also attached to this stage is a motorized horizontal translation stage capable of supporting two cameras. A CCD camera used for astronomical observations occupies one camera position. The second position is used for the lidar detector.

3.2 Laser Launch Facility

The laser system consists of a Nd:YAG laser pumping a dye laser that is tuned to the sodium D_2 resonance line. The pump laser is a Spectra-Physics LAB-170-50 Nd:YAG frequency-doubled laser. It produces 210 mJ pulses at 50 Hz with a wavelength of 532 nm. The laser is cooled by a water-glycol mixture circulating through a refrigerating chiller. (Running water is not available at the remote site of the LZT.) An interlock system protects the laser from any failure of the cooling system.

The 532 nm radiation from the Nd:YAG pump laser is directed to a Cobra-Stretch CSTR-D-24-US dye laser that employs two 90 mm wide 2400 lines per mm gratings. This laser can be tuned from 330-710 nm and we operate it at 589 nm. Rhodamin 610, dissolved in Ethanol, is used as the dye medium. The resulting line width is 0.04 cm^{-1}, which corresponds to 1.2 GHz. The laser is equipped with a main amplifier that boosts its conversion efficiency to $\sim$50%. The resulting 10 ns pulses have an energy of $\sim$ 100 mJ. The output beam has a divergence of approximately 0.5 mrad. The beam profile is Gaussian with a "burn diameter" of approximately 4.5 $\times$ 2.8 mm. This corresponds to the diameter at which the intensity has fallen to about 2% (2.8 σ) of the central intensity. The standard deviation of the Gaussian beam along the two principal axes is thus 0.8 $\times$ 0.5 mm.

The wavelength of the output beam is monitored by a pulsed laser wavelength meter. This instrument uses a Fabry-Perot cavity and a CCD for precise wavelength measurement. The frequency accuracy is 0.02 cm^{-1} (600 MHz). A feedback loop is used to control the dye laser, maintaining frequency stability.

The main laser beam is expanded to $\sim$12 cm diameter by means of a concave diverging lens and launch telescope. The launch telescope is a refracting telescope with a 15 cm clear aperture and a focal length of 1100 mm, located with the lasers and the laser conditioning optics on the optical bench. The beam divergence can be varied from a diffraction limited parallel beam to several arcmin (the maximum field of view of the lidar detector is 0.7 arcmin) by varying the distance between the diverging lens and the objective lens of the launch telescope. No spatial filter is employed due to the high power of the beam, which would cause an air breakdown at the pinhole location.

The collimated beam produced by the launch telescope is directed to a 25 cm flat mirror mounted on an gimbal stage. This allows the uplink beam to be directed vertically with arcsec precision. The direction of the beam is monitored by a 15 cm Schmidt-Cassegrain telescope equipped with a CCD detector, which images the resulting LGS.

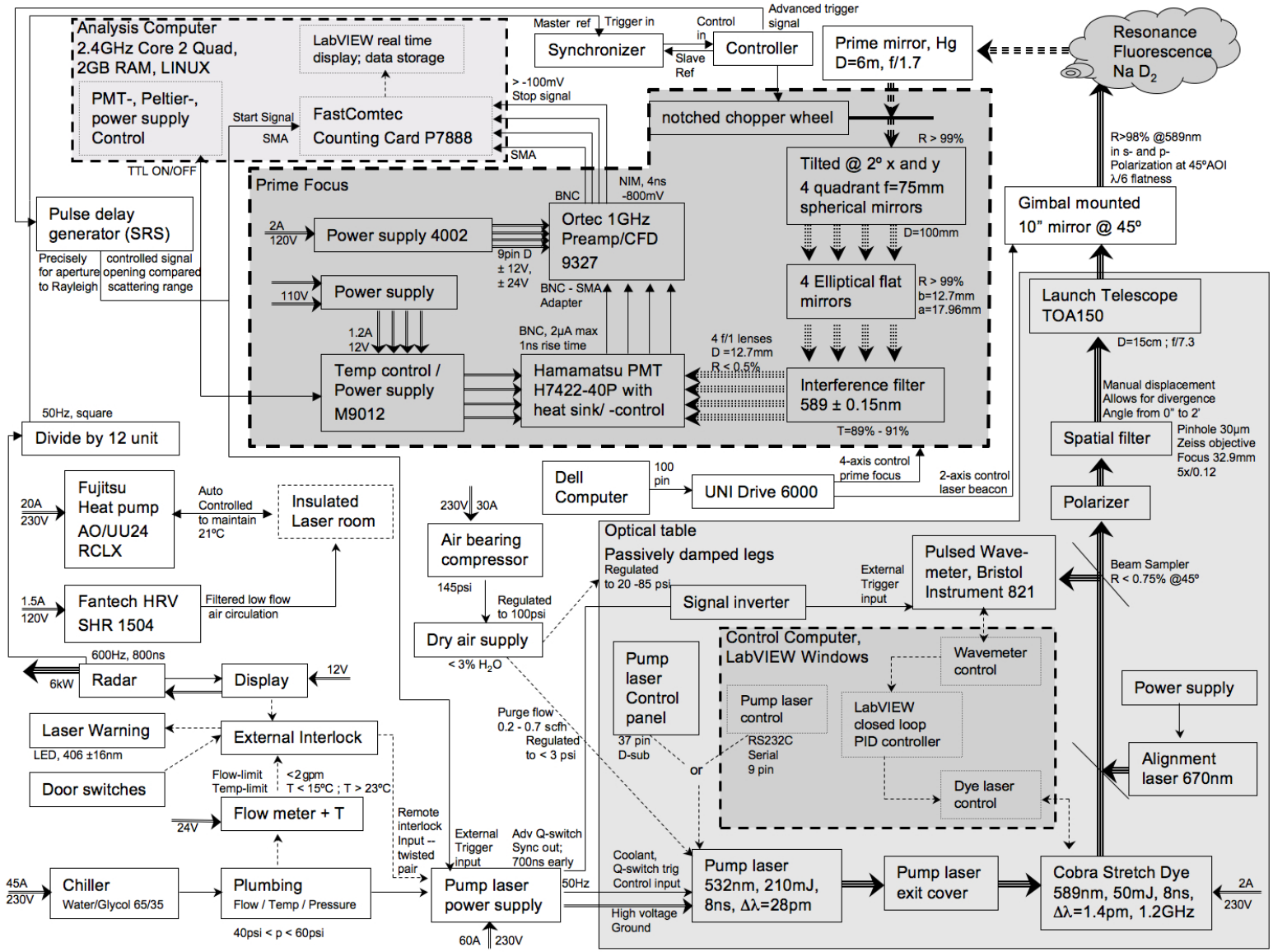

Figure 2. UBC LIDAR system design block diagram

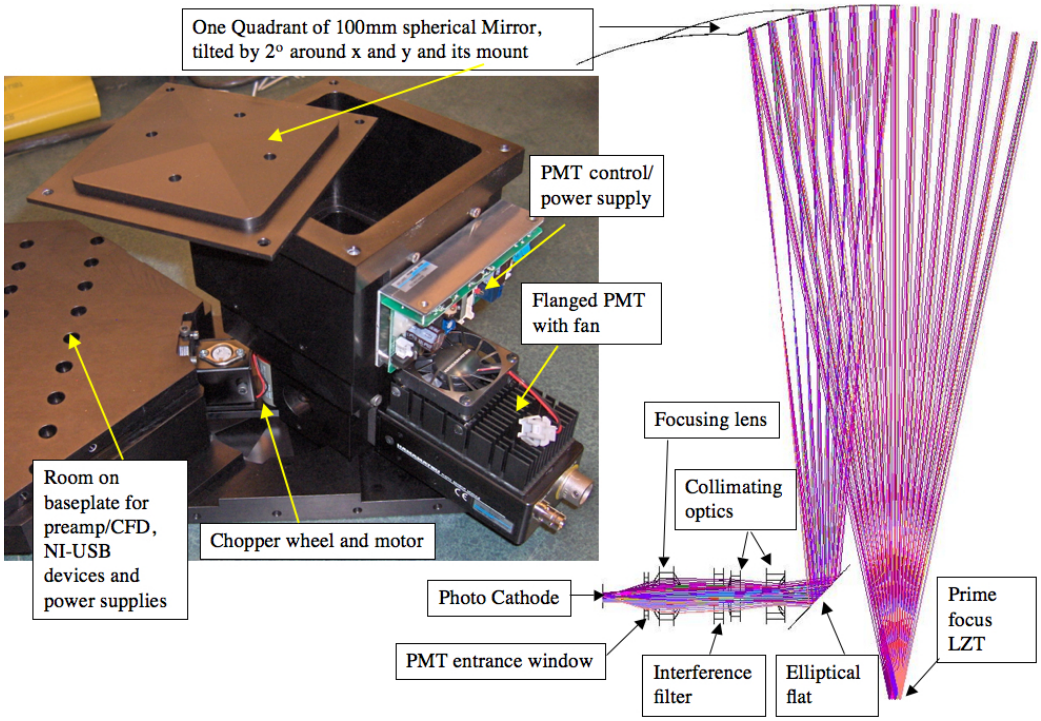

Figure 3. Ray trace of one of four sectors of the receiver system. Light expanding from the LZT prime focus is refocussed by four off-axis spherical mirror quadrants (one is shown), collimating optics, interference filter and focusing lens onto four photomultipliers (one photocathode is shown). In the picture the partly-assembled detector with one PMT. The support plate for the quadrant mirror, shown upside down, can be seen resting on top of the housing.

3.3 Receiver Optics and Electronics

The lidar detector consists of a chopper wheel, quadrant mirror, reimaging system, and four photomultiplier (PMT) detectors. The chopper wheel, located at the prime focus, protects the PMTs from the bright Rayleigh-scattered light from the uplink beam. The chopper employs a rotating wheel with two cut-outs. The position of the wheel is sensed by a phototransistor, which generates a pulse just before the beam is unblocked. The pulse triggers the laser after an adjustable digital delay. This allows us to set the range of the Rayleigh light that is blocked and ensure that none of the sodium light is lost.

The quadrant mirror is a concave spherical mirror, cut in four quadrants and reassembled with each part tilted slightly off axis. Located in the expanding beam above the prime focus, it splits the light into four equal parts. Each of the resulting four beams then enters a separate optical and detector system. These include lenses that re-image the pupil onto the photocathode, a narrowband filter, and a high-sensitivity PMT. The narrow-band filter is a flat interference filter with 90% central transmission and 260 pm FWHM centered at 588.995 nm. Its purpose is to block background light that is not at the sodium wavelength. In Figure 3, a ray trace of the optical system and a photograph of the partly-assembled detector are shown. The other PMTs are located at 90-degree intervals around the telescope axis on the detector mount.

The PMTs are equipped with GaAsP photo detectors, having a quantum efficiency of 37% at 589 nm. To reduce dark current, the PMTs are thermoelectrical cooled to a temperature of -5°C. The PMT output is connected to a 1 GHz preamplifier and constant fraction discriminator. Digital pulses, with 4-ns pulse width, produced by the discriminator are transferred from the prime focus to the data acquisition and control computer, located in the LZT control room ∼15 m away.

A four-channel multiscaler counting card records the arrival times of the incoming pulses, with respect to a timing pulse produced by the pump laser when it fires. These are binned in 2 ns intervals, which correspond to

0.3-meter vertical resolution. The system is controlled by a LabVIEW program running on a PC using a Linux operating system.

3.4 Safety Components and Trigger Circuit

The high peak power of the laser requires a system for the protection of aircraft crew and passengers against accidental exposure to the beam. A radar is used to detect approaching aircraft and automatically turn off the laser. For this purpose, we modified a commercial radar in a manner similar to that of Duck 2005.[6] The radar system is connected to the laser interlock system so that any target appearing on the radar immediately shuts down the laser. The system was verified by fly-over tests.

4. EXPECTED SYSTEM PERFORMANCE

Our laser emits at maximum 100 mJ per pulse (with an average power of 5 W and peak power of 10 MW per pulse). At a mean air-wavelength of 588.995 nm, this corresponds to $3{\cdot}10^{17}$ photons. The uplink efficiency is 60%, assuming 70% transmission through the atmosphere. This means $1.8{\cdot}10^{17}$ photons arrive at the sodium layer at each pulse. The convolution of the laser line profile and the Sodium hyperfine lines results in a scattering cross section of $6{\cdot}10^{-16}$ cm^2. The average number of photons per pulse is obtained by multiplying this cross section by the column density. We use a volume density[4] of $4{\cdot}10^{9}$ m^{-3}, which, when multiplied over an estimated layer thickness of 10 km gives a column density of $4{\cdot}10^{13}$ m^{-2}. The scattering probability is therefore 2.4% and $4.4{\cdot}10^{15}$ photons are scattered into 4π sterad. Our 6 m mirror has a collection probability of $2.8{\cdot}10^{-10}$ at the average range of 90 km from the scattering process and together with an assumed air transmission of 70%, $8.6{\cdot}10^{5}$ photons arrive on the mirror. The receiver's optical transmittance is 45%, including obscuration and the transmission of all optics. The PMTs have a photocathode sensitivity of 174 mA W^{-1}, which translates at 589 nm to a quantum efficiency of 37%. The overall receiver efficiency is therefore 16.6% and the number of photons received by the system is $1.4{\cdot}10^{5}$.

The telescope pupil is divided into four quadrants (see Section 3.3) with parallel detection lines in order to reduce coincidence losses. The fraction of photons detected is given by

$$\varepsilon = \frac{1}{1 + \tau_{CFD} f_i}\,, \tag{6}$$

where f_i is the photon arrival rate and τ_{CFD} is the deadtime of the constant-fraction discriminator (CFD). With a mean incoming photon rate $f_i = 530$ MHz (incident photons arrive over a range of order $t = 2 \cdot 10$ km$/c = 66$ μs), and $\tau_{CFD} \approx$5 ns, approximately 27% of the incident photons will be detected. Thus a total of $\sim 4{\cdot}10^{4}$ photons are detected from each pulse. With a bin size of 2 m, an average of $\sim$8 photons will be detected within in each bin.

The mean height of the sodium is given by

$$\overline{z} = \frac{1}{N} \sum N_i z_i\,, \tag{7}$$

where N_i is the number of photons received the i-th bin, centered at height z_i and $N = \sum_i N_i$. The variance in the mean height is therefore

$$Var(\overline{z}) = \frac{1}{N^2} \sum \left[(z_i - \overline{z})^2 N_i \right]\,. \tag{8}$$

For illustration, suppose that the density of the sodium layer is constant in a uniform layer of thickness w centered at height $\overline{z}$ and zero above and below this layer. We divide the layer into $2m+1$ equal bins, so $z_i = \overline{z} + w(i-m)/(2m+1)$ and the expected number of photons in each bin is $N_i = N/(2m+1)$. Inserting this into Equation (8) gives

$$Var(\overline{z}) = \frac{2w^2}{N(2m+1)^3} \sum_{i=1}^{m} i^2 = \frac{m(m+1)}{3N(2m+1)^2} w^2\,. \tag{9}$$

The 1σ uncertainty in the mean height is therefore

$$\sigma(\overline{z}) = \sqrt{\frac{m(m+1)}{3N(2m+1)^2}}\; w \approx \frac{w}{\sqrt{12N}}\,. \tag{10}$$

Taking $w = 10$ km and $N = 4{\cdot}10^4$, we expect the 1σ uncertainty in the mean height, from a single laser shot, to be approximately 14 m. If we were to average 50 shots, we would obtain 1σ uncertainty of 2 m on a timescale of 1 sec. For comparison, the RMS height fluctuation for frequencies above 1 Hz, obtained by integrating Equation (3), is 4 m. Averaging the sodium profiles reduces the time resolution. This is not what we want. Rather, it would be better to average many power spectra taken at the 50 Hz sampling rate in frequency space. The observed mean height $h_0(t)$, at time t, can be written as

$$h_0(t) = h(t) + r(t)\,, \tag{11}$$

where $h(t)$ is the true mean height and $r(t)$ is the random error due to the photon noise. Taking the Fourier transform of this equation and squaring, we obtain

$$|H_0(\nu)|^2 = [H(\nu) + R(\nu)]\,[H(\nu) + R(\nu)]^* = |H(\nu)|^2 + |R(\nu)|^2 + H(\nu)R^*(\nu) + H^*(\nu)R(\nu)\,. \tag{12}$$

The quantity on the left is the power spectrum of the observed data. On the right we have the true power spectrum of sodium mean height fluctuations, to which is added the power spectrum of the photon noise plus two fluctuating quantities whose mean is zero. If we now average many such spectra, taken minutes, hours or days apart, the fluctuating quantities will average to zero. Thus

$$\left\langle |H_0(\nu)|^2 \right\rangle = \left\langle |H(\nu)|^2 \right\rangle + \left\langle |R(\nu)|^2 \right\rangle\,. \tag{13}$$

We see that the averaged power spectrum is the sum of the true power spectrum plus the power spectrum of the noise. Since the photon noise has no temporal or spatial correlations, this component will have a flat power spectrum. Its amplitude is known since the number of photons is known. So, by subtracting a flat spectrum of the appropriate amplitude, we can recover the true power spectrum of the mean height with a 50 Hz time resolution.

5. STATUS AND OBSERVING PROGRAM

At the time of writing, the lidar system has been installed at the LZT and is undergoing calibration and testing. First light is expected in early June. The system will be operated on clear nights over a one-year period to allow the yearly cycle of sodium variability to be studied. Our first-light image of the laser launch is shown in Figure 4. We expect that initial results will be released in the third quarter of 2008, and that a full analysis will be completed by the end of the observing program in mid 2009. In general, one night of data suffices to generate a power spectrum of the mean height variability, covering the frequency range of interest to TMT AO systems. As described above, data from many nights can be averaged in frequency space to improve the signal-to-noise ratio, especially on the low frequency side of the spectrum.

The performance of the system is presently limited by our counting card, which has a maximum continuous count rate of only 21 MHz. This limits the number of photons that can be detected to ∼1500 photons per shot, about one thirtieth of the expected number that would be received at full laser power. A new card that will allow count rates of up to 2 GHz is expected to be available soon. Upgrading the system with this card will provide an increase of more than a factor of five in signal-to-noise ratio and will allow the lidar to achieve its full potential.

ACKNOWLEDGMENTS

Funding for this work was provided by grants from the Natural Sciences and Engineering Research Council of Canada, the Canada Foundation for Innovation, and the British Columbia Knowledge Development Fund. TP gratefully acknowledges support from the German Academic Exchange Service (DAAD). We have benefited from frequent interaction and discussion with the TMT, Herzberg Institute of Astrophysics and University of Victoria AO teams.

Figure 4. First light of the laser launch facility. On the left hand site, parts of the stabilizing spider of the 6-m mirror, the hexapods of the prime focus, the 25 cm flat and the safety radar as well as the lidar beam are visible. On the right hand at the bottom, the laser room in action is shown and the LZT enclosure with the uplink beam and a partly opened roof is visible in the upper part. The blue light is caused by the laser warning LEDs.

REFERENCES

[1] Davis, D. S., Hickson, P., Herriot, G., and She, C.-Y., "Temporal variability of the telluric sodium layer," *Opt. Lett.* **31**(22), 3369–3371 (2006).

[2] Herriot, G., Hickson, P., Ellerbroek, B., Véran, J.-P., She, C.-Y., Glare, R., and Looze, D. *Proc. SPIE* **6272**, 46 – 55 (2006).

[3] Ellerbroek, B., Adkins, S., Andersen, D., Atwood, J., Boyer, C., Byrnes, P., Conan, R., Gilles, L., Herriot, G., Hickson, P., Hileman, E., Joyce, D., Leckie, B., Liang, M., Pfrommer, T., Sinquin, J.-C., Véran, J.-P., Wang, L., and Welle, P. *Proc. SPIE this conference [7015-26]* (2008).

[4] She, C. Y., Yu, J. R., Latifi, H., and Bills, R. E., "High-spectral-resolution fluorescence light detection and ranging for mesospheric sodium temperature measurements," *Appl. Opt.* **31**(12), 2095 (1992).

[5] Hickson, P., Pfrommer, T., Cabanac, R., Crotts, A., Johnson, B., de Lapparent, V., Lanzetta, K., Gromoll, S., Mulrooney, M., Sivanandam, S., and Truax, B., "The large zenith telescope – a 6-meter liquid-mirror telescope," *Publications of the Astronomical Society of the Pacific* **119** (2007).

[6] Duck, T. J., Firanski, B., Lind, F. D., and Sipler, D., "Aircraft-protection radar for use with atmospheric lidars," *Appl. Opt.* **44**(23), 4937–4945 (2005).